

光学学报

基于光纤布拉格光栅对的双波长线形腔掺铒光纤激光器设计与优化

张振鹤, 刘丰年*, 果鑫, 陈涛, 韩林桀

湖南工业大学计算机学院, 湖南 株洲 412007

摘要 基于光纤布拉格光栅对(DFBGs)的双波长线形腔光纤激光器利用偏振烧孔效应实现双波长激光稳定输出的研究颇多,但有关3 dB光纤环形镜(FLM)与光纤布拉格光栅(FBG)构成腔镜或仅FBG构成腔镜,以及DFBGs的选择对其激光输出性能[光信噪比(OSNR)、斜率效率及稳定性等]的影响的研究很少。本文实验首先在双波长线形腔掺铒光纤激光器中比较了3 dB FLM与FBG构成腔镜和仅FBG构成腔镜的双波长激光的输出性能,结果表明,仅FBG构成腔镜的输出性能优于3 dB FLM与FBG构成腔镜的输出。其次在仅FBG构成腔镜的线形腔中对低反射率FBG(输出镜)反射率相同与不同时的输出性能进行了对比,研究表明,低反射率FBG的反射率相同时双波长激光输出具有较高的OSNR、斜率效率和稳定性。接着改变构成腔镜的两对FBG的中心波长间隔分别为4、8、12 nm,研究表明,中心波长间隔越大输出越稳定,OSNR越高,但激光器的斜率效率有所降低。最后在室温环境下实现了两个激光波长分别为1550 nm和1562 nm,OSNR分别为50.24 dB和51.19 dB左右,中心波长变化分别小于0.030 nm和0.035 nm,输出功率波动分别小于0.061 mW和0.059 mW,3 dB带宽分别为~0.146 nm和~0.144 nm的稳定输出,该结果为线形腔双波长的更优输出。

关键词 光纤布拉格光栅对; 偏振烧孔; 3 dB光纤环形镜; 双波长线形腔掺铒光纤激光器; 中心波长间隔

中图分类号 TN242 文献标志码 A

DOI: 10.3788/AOS231358

1 引言

目前,提高现代光纤通信系统的通信容量最直接的方式就是基于波分复用技术采用多个单波长激光器作为光源。但是单纯地增加光源数量,会增加成本,因此性能稳定的多波长光纤激光器^[1-3]受到人们的广泛关注。同时多波长光纤激光器也在多维信息光纤传感方面有着潜在的应用。多波长掺铒光纤激光器(EDFL)在室温下的稳定运行面临如下问题:由于掺铒光纤(EDF)的均匀增益展宽,极易导致模式竞争,尤其在激光波长间隔较窄的情况下会使得多波长激光器的稳定性更差^[4]。

目前已报道多种抑制模式竞争实现多波长激光器的方案。例如,双相移光纤布拉格光栅(FBG)与切趾FBG结合的结构^[5]、法布里-珀罗滤波器与可调节的窄带FBG结合的结构^[6]、基于光纤环形镜(FLM)的结构^[7-8]以及其与马赫-曾德尔干涉仪结合的结构^[9]、非对称两级保偏光纤的萨格纳克环滤波器结构^[10]、基于保偏FBG和马赫-曾德尔干涉仪滤波器的结构^[11]、利用可变光衰减器调节腔内损耗^[12]、用特殊材料作为可饱和吸收体^[13]、用液氮冷却^[14],以及采用光纤布拉格光栅对(DFBGs)^[15-18]等方案。虽然这些方法可以实现多波长的稳定输出,但难以同时满足结构简单、成本低的要求,也未对激光器的结构、输出功率、光信噪比(OSNR)以及稳定性进行对比分析。

EDF属于均匀加宽的工作物质,铒离子对谱线不同频率处的增益都有贡献,会在谱线中形成多个模式。本文基于线形腔结构,利用偏振烧孔(PHB)效应,通过调整三环机械偏振控制器(PC)的三个波片来改变EDFL中不同波长光的偏振态(偏振方向、角度和幅值),使腔内与波长相关的增益和损耗发生变化,进而选择合适的DFBGs实现稳定的双波长激光输出。本文实验首先比较了FLM和高反射率FBG(HR-FBG)分别作为全反镜,低反射率FBG(LR-FBG)作为输出镜的激光输出。结果表明,利用HR-FBG作为全反镜的激光输出光谱性能相对于FLM更优。接着在EDFL中采用两个相同反射率的HR-FBG作为全反镜,比较两个LR-FBG作为输出镜时反射率相同与不同的输出情况,研究表明,采用两个LR-FBG的反射率相同时,双波长激光输出优于反射率不同情况下的输

收稿日期: 2023-08-04; 修回日期: 2023-09-13; 录用日期: 2023-09-20; 网络首发日期: 2023-10-23

基金项目: 湖南省自然科学基金(省市联合)(2022JJ50067, 2021JJ50049)、湖南省教育厅科学研究一般项目(21C0405)

通信作者: *836354185@qq.com

出。最后在前两组实验的基础上,对DFBGs不同中心波长间隔的输出情况进行对比,结果表明,DFBGs中心波长间隔大的输出OSNR高于中心波长间隔较窄时的输出,同时双波长输出也更为稳定。与现有的PHB方案^[19-22]相比,该激光器具有结构简单紧凑、成本低、稳定性良好等优点。

2 原 理

2.1 FLM的结构及原理

FLM的结构图如图1所示,FLM可由 1×2 耦合器(coupler)或者 2×2 coupler将两个输出端口熔接形成光纤环构成。

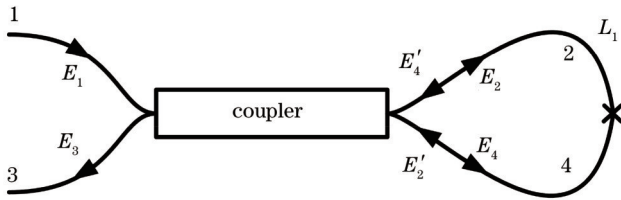


图1 FLM的结构图

Fig. 1 Structure diagram of FLM

当入射光进入coupler后分成具有 $\pi/2$ 相位延迟沿顺时针和逆时针传输的两束光,有

$$r_1=2i\sqrt{K(1-K)}(1-\gamma)\exp[(-\alpha+i\beta)L_1], \quad (1)$$

$$t_1=(1-2K)(1-\gamma)\exp[(-\alpha+i\beta)L_1], \quad (2)$$

式中: K 为coupler耦合比; L_1 为光纤环长度; r_1 和 t_1 分别为FLM的反射系数和透射系数; γ 为coupler的附加损耗; α 为圈中任一方向的单程衰减系数(即传输损耗和熔接损耗); β 为光纤的传播常量。将式(1)和式(2)求模平方可得

$$R=4K(1-K)(1-\gamma)^2\exp(-2\alpha L_1), \quad (3)$$

$$T=(1-2K)^2(1-\gamma)^2\exp(-2\alpha L_1), \quad (4)$$

式中, R 和 T 分别为FLM的强度反射率和强度透射率,由于coupler具有对称性,则有

$$\begin{pmatrix} P_r \\ P_t \end{pmatrix} = (1-\gamma)^2 \exp(-2\alpha L_1) \begin{pmatrix} 4K(1-K) & (1-2K)^2 \\ (1-2K)^2 & 4K(1-K) \end{pmatrix} \begin{pmatrix} P_{in} \\ 0 \end{pmatrix}, \quad (5)$$

式中: P_{in} 为输入功率; P_r 为反射光功率; P_t 为透射光功率。由于光纤熔接过程中会带来损耗,因此有

$$\alpha_1^{abs}=1-(R+T)=1-(1-\gamma)^2\exp(-2\alpha L_1), \quad (6)$$

式中, α_1^{abs} 为吸收系数,表示由FLM引起的损耗。由于熔锥法制成的光纤耦合器附加损耗非常小,且当光纤环的半径足够大时,FLM中的弯曲损耗可以忽略不计,此时有

$$\alpha_1^{abs}=\gamma=\alpha=0, \quad (7)$$

将式(7)代入式(3)~(5)中可得

$$\begin{cases} R=4K(1-K), \\ T=(1-2K)^2, \end{cases} \quad (8)$$

$$\begin{pmatrix} P_r \\ P_t \end{pmatrix} = \begin{pmatrix} 4K(1-K)P_{in} \\ (1-2K)^2P_{in} \end{pmatrix}. \quad (9)$$

根据式(9)画出 P_r 和 P_t 与 K 的关系变化曲线如图2所示。当 $K=0.5$ 时, $P_r=P_{in}$, $P_t=0$,即FLM起到全反射镜的作用;当 $K=0$ 或 1 时, $P_r=0$, $P_t=P_{in}$,即FLM起到全透射镜的作用。

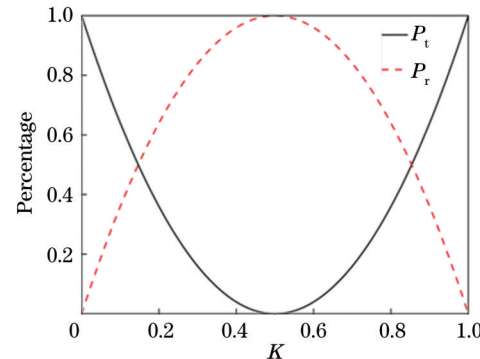


图2 P_t 和 P_r 随 K 的变化曲线

Fig. 2 Variation curves of P_t and P_r with K

实际上,coupler的耦合比不能完全做到50%,当 $K\neq 0.5$ 时,FLM中会存在自相位调制,则入射光场 E_1 从1端口进入,经过光纤环之后会产生相移 $\varphi=2\pi n|E_1|^2L_1/\lambda$,其中 n 为非线性克尔系数, λ 为入射光波长。入射光场 E_1 进入coupler之后的光场 E_2 和 E_4 分别为

$$\begin{cases} E_2=\sqrt{K}E_1 \\ E_4=i\sqrt{1-K}E_1 \end{cases}, \quad (10)$$

光场 E_2 和 E_4 在FLM中环行一周后,变为

$$\begin{cases} E'_2=\sqrt{K}E_1\exp(iK\varphi) \\ E'_4=i\sqrt{1-K}E_1\exp[i(1-K)\varphi] \end{cases}. \quad (11)$$

则3端口输出光场的表达式为

$$E_3=\sqrt{K}E'_2+i\sqrt{1-K}E'_4, \quad (12)$$

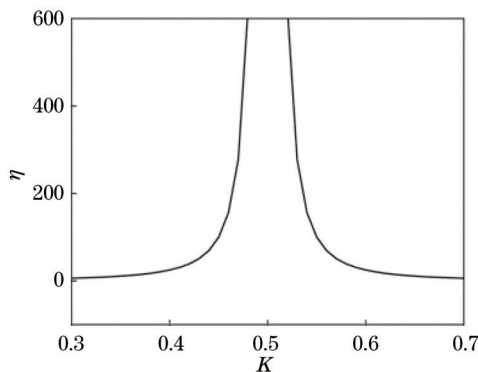
其输出光强表达式为

$$|E_3|^2=E_3\bullet E_3^*=\left|E_1\right|^2\left\{1-2K(1-K)\bullet\left\{1+\cos[(1-2K)\varphi]\right\}\right\}. \quad (13)$$

设 $\varphi=m\pi/(1-2K)$,则有 $m=2k+1(k=0,1,2,\dots)$ 时,3端口输出光强最大为 $|E_1|^2$; $m=2k(k=0,1,2,\dots)$ 时,3端口输出光强最小为 $|E_1|^2(1-2K)^2$ 。1端口的反射光强 $|E_1|^2$ 与3端口的输出光强 $|E_3|^2$ 的比值 $\eta=1/(1-2K)^2$,如图3所示。当 $K\approx 0.5$ 时, η 趋于无穷大,1端口的反射光远大于3端口的透射光,则FLM可以作为全反射镜用于EDFL的设计。

2.2 PHB效应的原理

由于EDF是一种均匀加宽的工作物质,其增益特性会导致多个模式中较弱的模式被强光抑制即增益,

图3 反射光强与输出光强比值 η 随 K 的变化曲线Fig. 3 Variation curves of η ($|E_1|^2/|E_3|^2$) with K

一个模式振荡会抑制其他模式的光出现(即模式竞争^[23])。EDF中不同的 Er^{3+} 具有不同方向特性,腔内光子经过EDF时,只有 Er^{3+} 偶极振子方向和腔内光子偏振态一致,才能引起部分偏振的受激辐射,结果表现为EDF可以根据腔内光子的偏振状态产生不同的响应。在EDF中,具有某一偏振态的光会引起对应偏振态的反转粒子集居数饱和,使得该偏振态增益下降,当该偏振态的强偏振光进入EDF,再用另一弱偏振光入射进行放大,由于偏振饱和效应,弱偏振光的偏振方向越靠近强偏振光,获得的增益越小,两个偏振光方向成 $\pi/2$ 时增益最大。

实验中采用工作在1550 nm波长的三环机械PC来控制两个波长光的偏振态^[24],三环机械PC的结构如图4所示。

图4中 θ_1 、 θ_2 和 θ_3 分别为PC各波片的应力诱导双

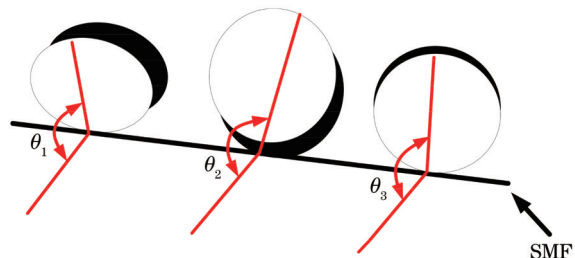


图4 三环机械PC结构图

Fig. 4 Structure diagram of three-ring mechanical polarization controller (PC)

折射轴与单模光纤(SMF)的x轴之间的夹角。 θ_i 是一个随机变量,均匀分布在0到 π 的范围内。PC中缠绕SMF,三个波片中光纤圈数为2/4/2,分别等效为1/4波片、1/2波片和1/4波片,用于控制相位延迟。PC中各波片的传输矩阵可表示为

$$T_i = R_i \begin{bmatrix} 1 & 0 \\ 0 & \exp(i\varphi_i) \end{bmatrix} R_i^*, \quad (14)$$

式中, φ_i 是PC各个波片引入的相位延迟,旋转矩阵 R_i 表示为

$$R_i = \begin{bmatrix} \cos \theta_i & \sin \theta_i \\ \sin \theta_i & -\cos \theta_i \end{bmatrix}, \quad (15)$$

式中, R_i 只与 θ_i 有关。入射光偏振态的调节是通过改变应力诱导双折射轴与SMF的x轴之间的夹角(即旋转PC波片)来完成的。PC的传输矩阵表示为

$$T_{\text{PC}}(\theta_1, \theta_2, \theta_3, \lambda) = T_1 \times T_2 \times T_3, \quad (16)$$

式中, T_1 、 T_2 和 T_3 为各波片的传输矩阵,其表达式为

$$T_i = \begin{bmatrix} \cos^2 \theta_i + \sin^2 \theta_i \exp(i\varphi_i) & \frac{1}{2} \sin 2\theta_i [1 - \exp(i\varphi_i)] \\ \frac{1}{2} \sin 2\theta_i [1 - \exp(i\varphi_i)] & \sin^2 \theta_i + \cos^2 \theta_i \exp(i\varphi_i) \end{bmatrix} \quad (i=1,2,3), \quad (17)$$

其中,

$$\varphi_1 = \varphi_3 = \frac{2\pi}{\lambda} \times \frac{1550}{4}, \varphi_2 = \frac{2\pi}{\lambda} \times \frac{1550}{2}. \quad (18)$$

式(17)和式(18)表明,通过控制PC波片角度变化可以改变不同波长光的传输矩阵,从而改变光的偏振态。设某一个波长光的输入向量为 E_{x1} 和 E_{y1} 分别表示在x和y轴上的分量,经过三环PC之后的输出向量为 E_{x2} 和 E_{y2} 。

$$\begin{bmatrix} E_{x2} \\ E_{y2} \end{bmatrix} = T_{\text{PC}}(\theta_1, \theta_2, \theta_3, \lambda) \begin{bmatrix} 1 & 0 \\ 0 & \exp\left(i\frac{2\pi BL}{\lambda}\right) \end{bmatrix} \begin{bmatrix} E_{x1} \\ E_{y1} \end{bmatrix}, \quad (19)$$

式中: B 为双折射系数; L 为激光器腔长; λ 为输入光的波长。因此通过调整PC的三个波片来改变EDFL中不同波长光的偏振态,可实现稳定的双波长激光输出。

3 实验装置

3.1 基于FLM结构的双波长线形腔EDFL的实验装置

如图5所示为基于FLM结构的双波长线形腔EDFL的实验结构。该EDFL由 1×2 的coupler构成FLM、两个中心波长不同的LR-FBG、机械三环PC和一段7 m长的EDF作为增益介质组成。EDF在980 nm处的吸收系数为6.5 dB/m,980 nm的泵浦光从FLM和EDF之间的波分复用器(WDM)送入腔内,PC在两个LR-FBG中间用于调整两个波长光的偏振态,抑制模式竞争,从而实现双波长激光的输出。

3.2 基于HR-FBG结构的双波长线形腔EDFL的实验装置

基于HR-FBG结构的双波长线形腔EDFL的实

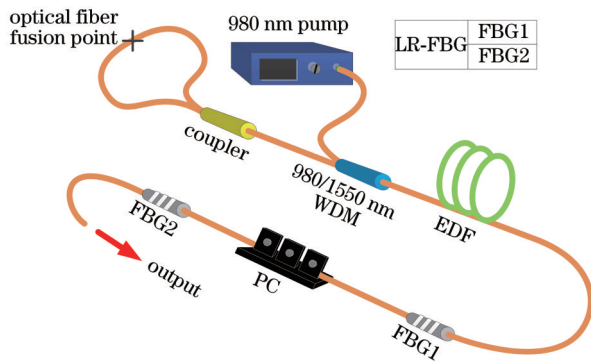


图5 基于FLM的EDFL结构图

Fig. 5 Structure diagram of EDFL based on FLM

验结构如图6所示。该EDFL将图5中的FLM更换成两个串联的高反射率($\sim 95\%$)的FBG,其中FBG1和FBG3、FBG2和FBG4的中心波长相同。通过调整在两个LR-FBG中间的PC,实现双波长激光的输出。

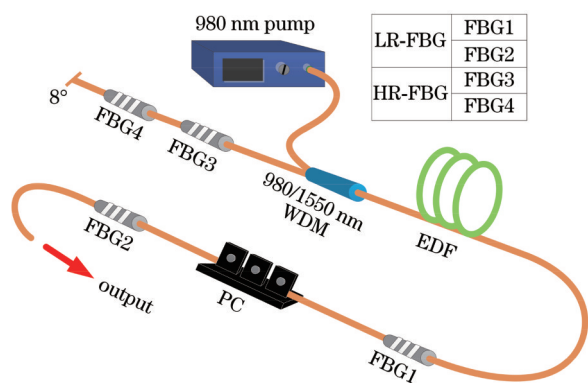


图6 基于HR-FBG的EDFL结构图

Fig. 6 Structure diagram of EDFL based on HR-FBG

4 结果与讨论

4.1 基于FLM和HR-FBG结构的双波长线形腔EDFL的对比分析

对于图5和图6的实验装置,FBG1和FBG2的中

心波长分别为1550 nm和1560 nm,反射率分别为45%和35%(通过OptiSystem仿真可得,LR-FBG反射率在30%~50%时,输出光谱质量更优。在此不再赘述);FBG3和FBG4的中心波长分别与FBG1和FBG2对应,反射率均为95%。如表1所示。

表1 基于FLM和HR-FBG结构的EDFL的FBG参数

Table 1 FBG parameters of EDL based on FLM and HR-FBG structures

	Experimental setup	Fig. 5	Fig. 6
FBG1	Center wavelength /nm	1550	1550
	Reflectivity /%	45	45
FBG2	Center wavelength /nm	1560	1560
	Reflectivity /%	35	35
FBG3	Center wavelength /nm	—	1550
	Reflectivity /%	—	95
FBG4	Center wavelength /nm	—	1560
	Reflectivity /%	—	95

实验测得的基于FLM和HR-FBG结构的双波长线形腔EDFL输出功率与泵浦功率的关系如图7(a)所示。图7(b)为通过分辨带宽0.2 nm的光谱分析仪(OSA)测量的两种结构的双波长激光输出光谱图。由图7分析可得,通过调节PC得到1550 nm和1560 nm双波长的激光输出,基于这两种结构的双波长线形腔EDFL的斜率效率基本相等,输出两个波长的OSNR均为50 dB以上,但由于FLM反射谱为宽带光谱^[25],对边模的抑制能力较差,HR-FBG结构中FBG反射光谱较窄^[26],能够实现选频,从而更好地抑制边模起振,所以基于HR-FBG结构的EDFL比基于FLM结构的EDFL的OSNR更高。因此,本文的后续实验均采用基于HR-FBG结构的双波长线形腔EDFL进行对比分析。

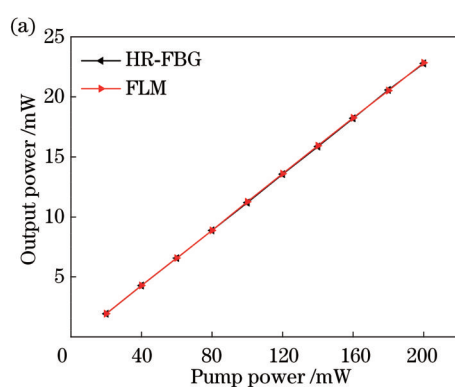


图7 FLM和HR-FBG结构的对比。(a) 输出功率与泵浦功率关系图;

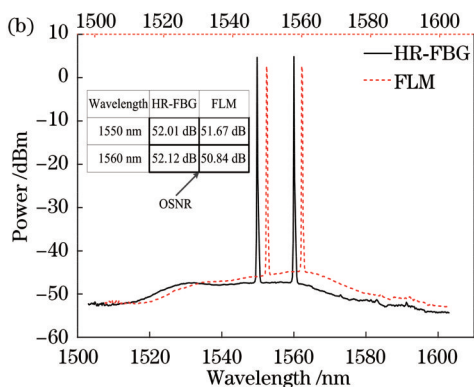


Fig. 7 Comparison of FLM and HR-FBG structures. (a) Relationship between output power and pump power; (b) dual-wavelength laser output spectra

4.2 基于双波长线形腔 EDFL 的 LR-FBG 反射率的对比分析

基于 HR-FBG 结构的 EDFL 中 LR-FBG 反射率对比实验的 FBG 参数如下:FBG1 和 FBG2 的中心波长分别为 1550 nm 和 1562 nm,FBG1 反射率为 45% 和 35% 两组,FBG2 反射率为 35%,FBG3 和 FBG4 的中心波长分别与 FBG1 和 FBG2 对应,反射率均为 95%。如表 2 所示。

实验分为两个 LR-FBG 反射率相同和不同两组。

表 2 基于 LR-FBG 反射率对比实验的 FBG 参数

Table 2 FBG parameters of comparison experiments based on LR-FBG reflectivity

	Number of experiments	①	②
FBG1	Center wavelength /nm	1550	1550
	Reflectivity /%	45	35
FBG2	Center wavelength /nm	1562	1562
	Reflectivity /%	35	35
FBG3	Center wavelength /nm	1550	1550
	Reflectivity /%	95	95
FBG4	Center wavelength /nm	1562	1562
	Reflectivity /%	95	95

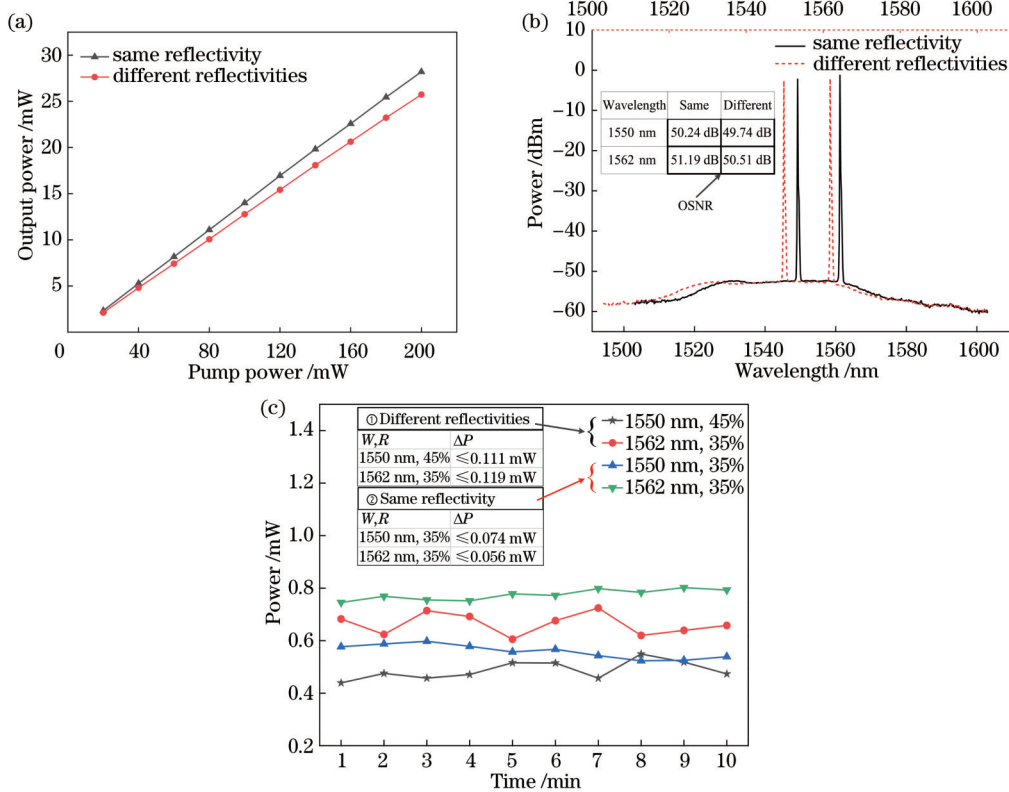


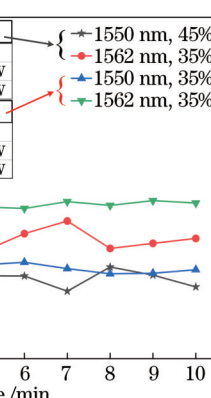
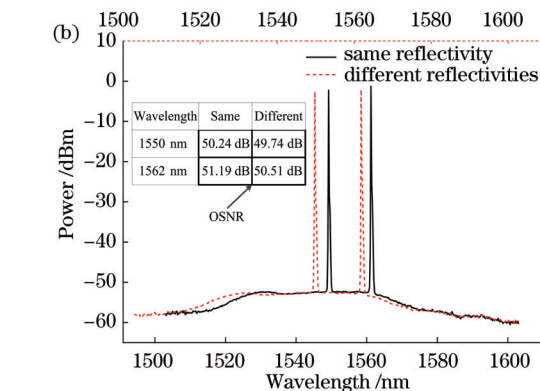
图 8 LR-FBG 反射率相同与不同时的对比。(a) 输出功率与泵浦功率关系图;(b) 双波长激光输出光谱图;(c) 输出功率的稳定性
Fig. 8 Comparison of same and different LR-FBG reflectivities. (a) Relationship between output power and pump power; (b) dual-wavelength laser output spectra; (c) stability of output power

如图 9(a)所示为实验测得的基于 HR-FBG 结构的 DFBGs 中心波长间隔分别为 4、8、12 nm 的双波长

测得 LR-FBG 反射率相同和不同的 EDFL 输出功率与泵浦功率的关系以及双波长激光输出光谱分别如图 8(a)和 8(b)所示。可见两个 LR-FBG 反射率相同时的 EDFL 斜率效率和 OSNR 比反射率不同时的更高。从输出功率稳定性分析,通过每隔 1 min 重复测量 10 次的双波长激光输出功率,获得两组实验 EDFL 的输出功率变化如图 8(c)所示,可得两组实验的功率波动均小于 0.12 mW,但反射率相同时的输出功率比不同时的更为稳定。这是由于两个 LR-FBG 反射率不同时,会导致两个波长的光信号在腔内的增益不均衡,可能会引起两个波长的模式竞争,导致其中一个波长的输出不稳定或受到抑制。因此,下述实验采用相同反射率的 DFBGs 进行。

4.3 基于双波长线形腔 EDFL 的 DFBGs 中心波长间隔的对比分析

基于 HR-FBG 结构的 EDFL 中 DFBGs 中心波长间隔对比实验的 FBG 参数如下:FBG1 的中心波长设置为 1550 nm,FBG2 中心波长依次设置为 1554、1558、1562 nm 的三组进行实验,FBG1 和 FBG2 的反射率均为 35%,FBG3 和 FBG4 的中心波长分别与 FBG1 和 FBG2 对应,反射率均为 95%。三组实验的 DFBGs 中心波长间隔 $\Delta\lambda$ 分别为 4、8、12 nm。如表 3 所示。



线形腔 EDFL 的输出功率与泵浦功率的关系图。三种波长间隔的双波长激光输出光谱图由分辨带宽

表3 基于HR-FBG结构的双波长线形腔EDFL的FBG参数

Table 3 FBG parameters of dual-wavelength linear cavity EDFL based on HR-FBG structure

Number of experiments		①	②	③
FBG1	Center wavelength /nm	1550	1550	1550
	Reflectivity /%	35	35	35
FBG2	Center wavelength /nm	1554	1558	1562
	Reflectivity /%	35	35	35
FBG3	Center wavelength /nm	1550	1550	1550
	Reflectivity /%	95	95	95
FBG4	Center wavelength /nm	1554	1558	1562
	Reflectivity /%	95	95	95
$\Delta\lambda$ /nm		4	8	12

0.2 nm的OSA测得,如图9(b)所示。测得的EDF放大自发辐射谱如图9(c)所示。由图9(a)和9(b)分析可知,当DFBGs的中心波长间隔逐渐增大时,双波长线形腔EDFL的斜率效率变高。但两个波长间隔太小会引起较强的模式竞争,从而导致波长间隔小的OSNR变低。因此,在设计双波长线形腔EDFL时,需要合理地选择波长才能实现更高的性能。

看出,与1550 nm波长的间隔越小,其对应波长的增益越高,最终表现为双波长线形腔EDFL的斜率效率变高。但两个波长间隔太小会引起较强的模式竞争,从而导致波长间隔小的OSNR变低。因此,在设计双波长线形腔EDFL时,需要合理地选择波长才能实现更高的性能。

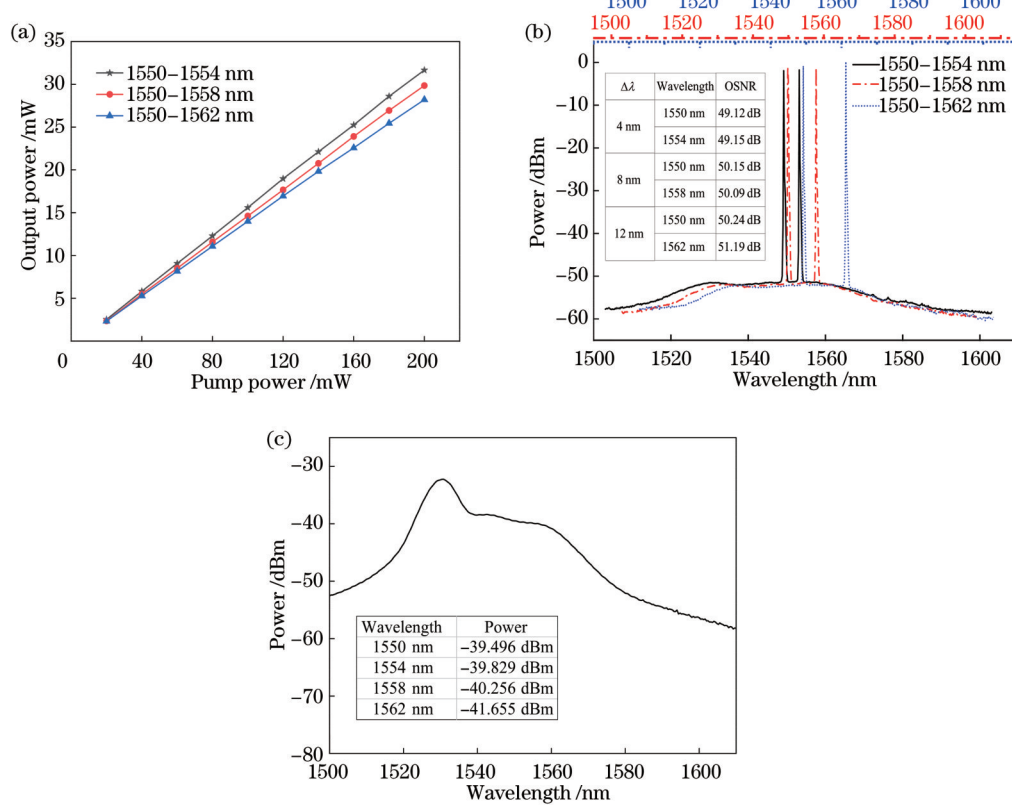


图9 基于HR-FBG结构的不同波长间隔对比。(a)输出功率与泵浦功率的关系图;(b)双波长激光输出光谱图;(c)EDF放大自发辐射谱

Fig. 9 Comparison of different wavelength intervals based on HR-FBG structure. (a) Relationship between output power and pump power; (b) dual-wavelength laser output spectra; (c) EDF amplified spontaneous emission spectrum

对双波长线形腔EDFL的长期稳定性进行分析,通过每隔10 min重复扫描10次获得随时间变化的双波长激光输出光谱,这些结果由分辨带宽为0.2 nm的OSA进行测量。DFBGs中心波长间隔 $\Delta\lambda$ 分别为4、

8、12 nm的一系列双波长激光输出光谱如图10(a)、10(b)和10(c)的左图所示,可以看出,三种波长间隔的双波长激光输出光谱都不会随着时间的推移而跳变。接着对三种波长间隔的EDFL中心波长稳定性进

行分析, 测得其变化如图 10(a)、10(b) 和 10(c) 的右图所示, 可以看出, DFBGs 中心波长间隔 $\Delta\lambda$ 分别为 4、8、12 nm 时, 中心波长的变化都具有良好的稳定性。当 $\Delta\lambda$ 为 12 nm 时, 中心波长稳定性更好, 1550 nm 和 1562 nm 波长的激光中心波长变化分别为 ≤ 0.030 nm 和 ≤ 0.035 nm。三种波长间隔的 EDFL 双波长激光中心波长的波动随着中心波长的间隔增大而减小。

进一步对三种中心波长间隔的双波长激光输出功率稳定性和 3 dB 带宽进行分析, 通过光功率计和 OSA 分别对每个波长激光的输出功率和 3 dB 带宽进行 10

次测量(间隔 10 min), 最终得到三种波长间隔的各个波长激光的输出功率和 3 dB 带宽随时间的变化分别如图 11(a)、11(b) 和 11(c) 所示。可以得出, 随着 DFBGs 中心波长间隔逐渐增大, 双波长激光的输出功率和 3 dB 带宽波动逐渐减小。 $\Delta\lambda$ 为 12 nm 时, 1550 nm 和 1562 nm 波长激光的输出功率波动分别为 ≤ 0.061 mW 和 ≤ 0.059 mW, 3 dB 带宽分别为 ~ 0.146 nm 和 ~ 0.144 nm。上述结果表明, 对于基于 HR-FBG 结构的双波长线形腔 EDFL, DFBGs 的中心波长间隔越大, 两个模式之间的竞争越小, 输出的两个波长的激光更为稳定。

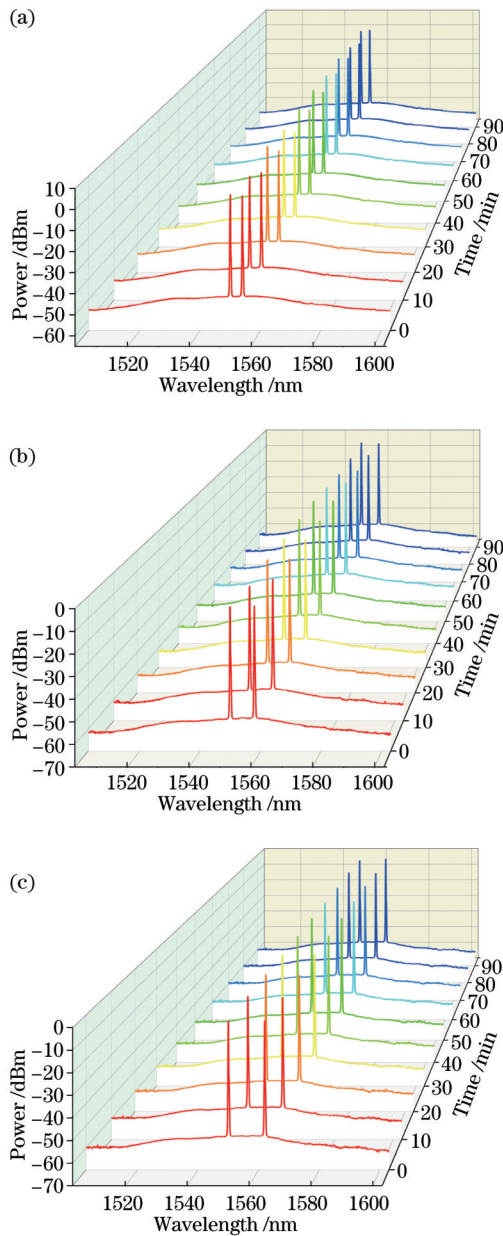


图 10 不同波长间隔下的激光输出光谱(左)和中心波长(右)的稳定性。(a) $\Delta\lambda=4$ nm; (b) $\Delta\lambda=8$ nm; (c) $\Delta\lambda=12$ nm
Fig. 10 Stabilities of laser output spectra (left) and center wavelengths (right) at different wavelength intervals. (a) $\Delta\lambda=4$ nm; (b) $\Delta\lambda=8$ nm; (c) $\Delta\lambda=12$ nm

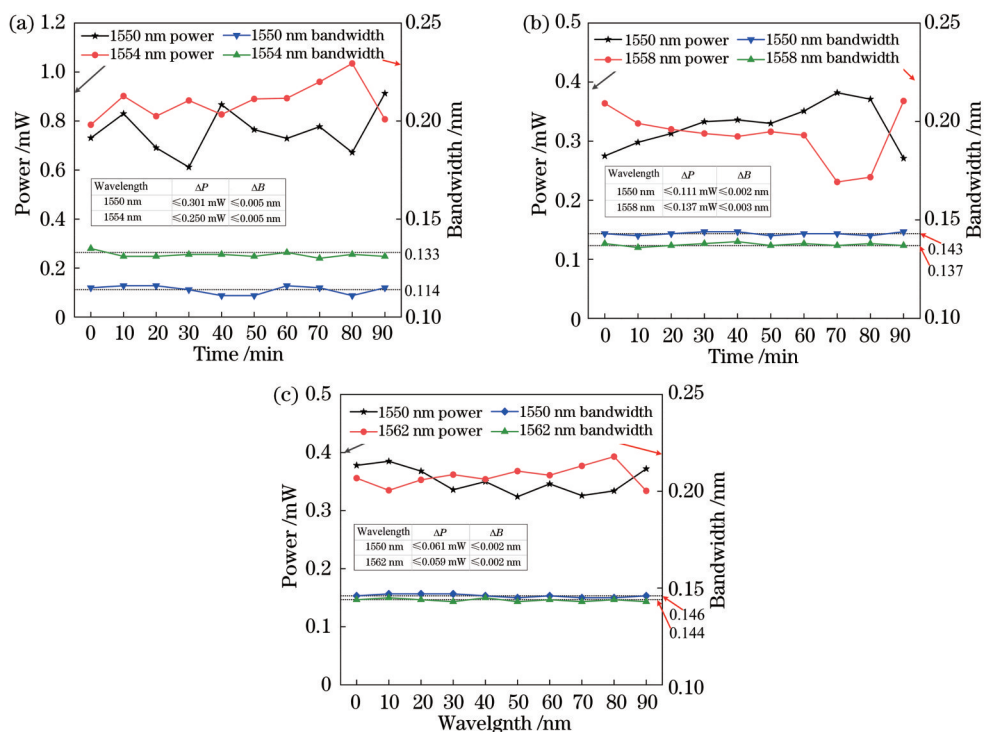


图11 不同波长间隔下的激光输出功率和3 dB带宽的稳定性。(a) $\Delta\lambda=4$ nm;(b) $\Delta\lambda=8$ nm;(c) $\Delta\lambda=12$ nm

Fig. 11 Stabilities of laser output power and 3 dB bandwidth at different wavelength intervals. (a) $\Delta\lambda=4$ nm; (b) $\Delta\lambda=8$ nm; (c) $\Delta\lambda=12$ nm

5 结 论

本文实现了一种结构简单的基于DFBGs的双波长线形腔EDFL,利用PHB原理在室温环境下能够输出稳定的双波长激光,并对其输出性能进行了对比分析。实验表明,采用HR-FBG作为全反镜时的输出优于FLM结构,且作为输出镜的两个LR-FBG反射率相同时,输出性能优于反射率不同的输出。研究还表明,随着DFBGs的中心波长间隔逐渐增大,EDFL的OSNR逐渐升高,双波长激光输出更稳定,但由于不同波长光在EDF中的增益差异,导致斜率效率有所降低。因此在设计双波长线形腔EDFL时,需要合理地选择FBG的中心波长、反射率等参数以及激光器的结构,以实现更高性能的输出。实验最终实现了1550 nm和1562 nm两个波长的OSNR分别为50.24 dB和51.19 dB左右、中心波长波动分别小于等于0.030 nm和0.035 nm、功率波动分别小于0.061 mW和0.059 mW、3 dB带宽分别为~0.146 nm和~0.144 nm的双波长线形腔EDFL。以上研究结果对室温条件下实现双波长激光输出的线形腔结构激光器的研究具有一定的参考价值。

参 考 文 献

- [1] 郭哲灿, 谢芳, 郭晓蕾, 等. 基于复合谐振腔的多波长窄线宽光纤激光器[J]. 激光与光电子学进展, 2022, 59(17): 1714008.
Guo Z C, Xie F, Guo X L, et al. Multi-wavelength and narrow linewidth fiber laser based on composite resonator[J]. Laser &
- [2] 韩冬冬, 张佳月, 高琼, 等. 可切换多波长全光纤被动锁模光纤激光器[J]. 光学学报, 2021, 41(5): 0506002.
Han D D, Zhang J Y, Gao Q, et al. Switchable multi-wavelength passively mode-locked all-fiber lasers[J]. Acta Optica Sinica, 2021, 41(5): 0506002.
- [3] 李思成, 许将明, 梁峻锐, 等. 波长间隔、幅度及数目可灵活调谐的多波长光纤激光器[J]. 中国激光, 2022, 49(13): 1316002.
Li S C, Xu J M, Liang J R, et al. Multi-wavelength fiber laser with adjustable wavelength interval, amplitude and number[J]. Chinese Journal of Lasers, 2022, 49(13): 1316002.
- [4] Zhang C F, Sun J, Jian S S. A new mechanism to suppress the homogeneous gain broadening for stable multi-wavelength erbium-doped fiber laser[J]. Optics Communications, 2013, 288: 97-100.
- [5] Yao Y, Chen X F, Dai Y T, et al. Dual-wavelength erbium-doped fiber laser with a simple linear cavity and its application in microwave generation[J]. IEEE Photonics Technology Letters, 2006, 18(1): 187-189.
- [6] He X Y, Fang X, Liao C R, et al. A tunable and switchable single-longitudinal-mode dual-wavelength fiber laser with a simple linear cavity[J]. Optics Express, 2009, 17(24): 21773-21781.
- [7] Wang M, Huang Y J, Yang J W, et al. Multi-wavelength mode-locked thulium-doped fiber laser based on a fiber-optic Fabry - Perot interferometer and a nonlinear optical loop mirror[J]. Laser Physics Letters, 2018, 15(8): 085110.
- [8] Drobyshev R V, Volikova A M, Lobach I A, et al. Multi-wavelength gain-switched Yb-doped fiber laser[J]. Laser Physics Letters, 2020, 17(6): 065102.
- [9] Torres-Gonzalez D, Sierra-Hernandez J M, Jauregui-Vazquez D, et al. An aluminum coated all-fiber mirror and a Mach-Zehnder interferometer for developing a switchable and tunable multi-wavelength laser[J]. Optics Communications, 2023, 537: 129397.

- [10] Zhou M, Luo Z Q, Cai Z P, et al. Switchable and tunable multiple-channel erbium-doped fiber laser using graphene-polymer nanocomposite and asymmetric two-stage fiber Sagnac loop filter[J]. Applied Optics, 2011, 50(18): 2940-2948.
- [11] He W, Li D, Zhu L Q, et al. Tunable multiwavelength erbium-doped fiber laser employing PM-FBG and Mach-Zehnder interferometer with optical fiber delay line[J]. IEEE Photonics Journal, 2017, 9(3): 7202108.
- [12] Wang S, Liu S H, Ni W J, et al. Dual-wavelength highly-sensitive refractive index sensor[J]. Optics Express, 2017, 25(13): 14389-14396.
- [13] Lau K Y, Bakar M H A, Muhammad F D, et al. Dual-wavelength, mode-locked erbium-doped fiber laser employing a graphene/polymethyl-methacrylate saturable absorber[J]. Optics Express, 2018, 26(10): 12790-12800.
- [14] Yamashita S, Yokooji M. Channel spacing-tunable sampled fiber Bragg grating by linear chirp and its application to multiwavelength fiber laser[J]. Optics Communications, 2006, 263(1): 42-46.
- [15] Wang H, Li Y G, Chen X D, et al. Highly efficient dual-wavelength ytterbium-doped fiber linear cavity laser based on cascaded fiber Bragg gratings[J]. Laser Physics, 2009, 19(6): 1257-1262.
- [16] Wang M, Chen C, Li Q, et al. Modulated dual-wavelength Er-doped fiber laser based on a semiconductor saturable absorber mirror[J]. Optical Fiber Technology, 2015, 21: 51-54.
- [17] Dong T H, Lin J Q, Gu C, et al. Switchable and tunable dual-wavelength passively mode-locked fiber laser[J]. Optical Fiber Technology, 2022, 68: 102750.
- [18] Wang M, Chen C, Li Q, et al. Photonic generation of tunable microwave signal using a passively Q-switched dual-wavelength fiber laser[J]. Microwave and Optical Technology Letters, 2015, 57(1): 166-168.
- [19] Feng S C, Xu O, Lu S H, et al. Single-polarization, switchable dual-wavelength erbium-doped fiber laser with two polarization-maintaining fiber Bragg gratings[J]. Optics Express, 2008, 16(16): 11830-11835.
- [20] Jiang P H, Shi C D, Fu S J, et al. Switchable and tunable dual-wavelength single-frequency fiber laser at 2050 nm based on saturable absorber[C]//Optica Advanced Photonics Congress 2022, December 11-15, 2022, Barcelona, Spain. Washington, D.C.: Optica Publishing Group, 2022: JTU6B.8.
- [21] Yan G X, Zhang W H, Li P, et al. Switchable and tunable linear cavity erbium-doped fiber laser based on FBGs embedded in Sagnac rings[J]. Laser Physics, 2022, 32(1): 015101.
- [22] Li K Y, Deng H Q, Yang C S, et al. Multi-wavelength, passively Q-switched, single-frequency fiber laser[J]. IEEE Photonics Technology Letters, 2019, 31(18): 1479-1482.
- [23] Pua C H, Norizan S F, Harun S W, et al. Non-membrane optical microphone based on longitudinal modes competition[J]. Sensors and Actuators A: Physical, 2011, 168(2): 281-285.
- [24] Zheng W J, Ruan S C, Zhang M, et al. Switchable multi-wavelength erbium-doped photonic crystal fiber laser based on nonlinear polarization rotation[J]. Optics & Laser Technology, 2013, 50: 145-149.
- [25] Feng S J, Mao Q H, Shang L, et al. Reflectivity characteristics of the fiber loop mirror with a polarization controller[J]. Optics Communications, 2007, 277(2): 322-328.
- [26] Othonos A. Fiber Bragg gratings[J]. Review of Scientific Instruments, 1997, 68(12): 4309-4341.

Design and Optimization of Dual-Wavelength Linear Cavity Erbium-Doped Fiber Laser Based on Double Fiber Bragg Gratings

Zhang Zhenhe, Liu Fengnian*, Guo Xin, Chen Tao, Han Linjie

College of Computer Science, Hunan University of Technology, Zhuzhou 412007, Hunan, China

Abstract

Objective Traditional single-wavelength fiber lasers make it challenging to meet the increasing capacity demands for modern optical fiber communication systems. Employing multiple single-wavelength fiber lasers as light sources by wavelength division multiplexing technology is bound to increase system complexity and costs. Additionally, there are potential applications in multi-dimensional information fiber sensing for multi-wavelength fiber lasers. Therefore, multi-wavelength fiber lasers with stable performance have been widely studied and can be adopted to expand communication systems and meet the needs of multi-dimensional information fiber sensing. However, the problems for stable operation of multi-wavelength erbium-doped fiber laser (EDFL) are as follows. At room temperature, due to the homogeneous broadening of erbium-doped fiber, it is easy to cause mode competition, which reduces the stability of multi-wavelength fiber lasers with narrow wavelength intervals. Based on the dual-wavelength linear cavity EDFL, we select a simple linear cavity fiber laser structure, optimize the reflectivity and center wavelength of fiber Bragg grating (FBG), and realize a stable dual-wavelength laser output by the polarization hole burning (PHB) effect. Compared with the existing PHB schemes, the laser features a simple and compact structure, low cost, and good stability. We hope that our study will help realize dual-wavelength linear cavity fiber lasers with excellent performance at room temperature.

Methods We study the influence of the structure of dual-wavelength linear cavity EDFL and FBG parameters (reflectivity and center wavelength) on the output performance of a dual-wavelength laser. Firstly, the output power and dual-wavelength laser spectra of 3 dB fiber loop mirror (FLM) and high reflectivity-FBG (HR-FBG) as the total reflector respectively, and low reflectivity-FBG (LR-FBG) as the output mirror are compared. Secondly, based on the double fiber

Bragg gratings (DFBGs) as a cavity mirror, two HR-FBGs with the same reflectivity are adopted as the total reflector. The output power, dual-wavelength laser spectra, and power stability with the same reflectivity and different reflectivities are compared when two LR-FBGs are utilized as the output mirror. Finally, based on the first two groups of experiments, DFBGs are leveraged to constitute the cavity, and the reflectivities of the two HR-FBGs and the two LR-FBGs are equal respectively. The output power and dual-wavelength laser spectra of DFBGs with different center wavelength intervals ($\Delta\lambda$ of 4, 8, and 12 nm) are compared. Additionally, the long-term laser stability is analyzed, which includes the temporal stability of spectra, center wavelength changes, power fluctuations, and 3 dB bandwidth stability.

Results and Discussions Firstly, the contrast experiment is carried out based on dual-wavelength linear cavity EDFL with FLM and HR-FBG structures. The results show that the slope efficiency of the two EDFL structures is basically equal. The optical signal-to-noise ratio (OSNR) based on the HR-FBG structure is still higher than that based on the FLM structure (Fig. 7), which indicates that the laser output performance of the linear cavity EDFL based on the HR-FBG structure is better. Secondly, in the dual-wavelength linear cavity EDFL based on HR-FBG structure, the influence of the same and different reflectivities of LR-FBG on the EDFL output performance is studied. The contrast experiment shows that the slope efficiency and OSNR of the two LR-FBGs with the same reflectivity are higher than those with different reflectivities, and the output power is more stable (Fig. 8). Finally, we study the effect of varying center wavelength intervals of DFBGs on the EDFL output performance. The contrast experiment shows that as the center wavelength interval of DFBGs gradually increases, the slope efficiency of the dual-wavelength linear cavity EDFL gradually decreases, and the OSNR of the two wavelength lasers gradually rises (Fig. 9). By adjusting the polarization controller (PC), the dual-wavelength laser output spectra of EDFL with three wavelength intervals will not hop with time. Constantly, the larger center wavelength interval leads to smaller center wavelength changes (Fig. 10), and smaller output power fluctuations and 3 dB bandwidth (Fig. 11).

Conclusions We realize a dual-wavelength linear cavity EDFL based on DFBGs with a simple structure and output a stable dual-wavelength laser at room temperature by the PHB effect, with the output performance analyzed. The results show that the output performance of the HR-FBG structure is better than that of the FLM structure. When the reflectivities of the two LR-FBGs adopted as the output mirror is the same, the output performance is better than that under different reflectivities. Additionally, as the center wavelength interval of DBFGs gradually increases, the OSNR of EDFL gradually improves, and the dual-wavelength laser output gradually stabilizes, but its slope efficiency will decrease due to the gain characteristics of EDF at different wavelengths. Finally, we realize that the stable results in dual-wavelength linear cavity EDFL with the OSNR of 1550 nm and 1562 nm are about 50.24 dB and 51.19 dB. The center wavelength fluctuations are less than 0.030 nm and 0.035 nm, and the power fluctuations are less than 0.061 mW and 0.059 mW, with 3 dB bandwidth of \sim 0.146 nm and \sim 0.144 nm respectively. The output results are better in the dual-wavelength linear cavity.

Key words double fiber Bragg gratings; polarization hole burning; 3 dB fiber loop mirror; dual-wavelength linear cavity erbium-doped fiber laser; center wavelength interval